Control Strategies for Neural Populations with Rectified Activation Function

Tommaso Menara Jorge Cortés

Abstract— **In the human brain, highly recurrent cortical circuitry supports information processing, coordinates learning episodes, and regulates healthy and diseased states. A key outstanding challenge of neural engineering is to ultimately control the collective dynamics of distinct neural populations, so as to promote the emergence or recovery of desired activity patterns. In this paper, we investigate the control of a general rate model of neural activity with rectified activation function. We first show that any target state in the open positive orthant can be reached in finite time. Furthermore, we present an array of results to perform (feedback and feedforward) efficient control in prototypical classes of networks with distinct connection types and in the case of sparse control inputs. Due to the relevance of rate models in both biological and artificial neural networks, our results lay the groundwork to enhance the dynamical behavior of *in vivo* and synthetic neural circuitry.**

I. Introduction

A quintessential objective of neural engineering is to understand how neural representation of external stimuli and internal spontaneous coordination produce actions relevant to a particular condition or situation [1], [2]. In this context, the design of authoritative control techniques for neuronal dynamics may have profound consequences in both the natural and artificial domains. In the former, targeted stimulation techniques may be used to restore desirable brain-wide activity patterns from diseased states [3], [4]. In the latter, untangling how external inputs drive the dynamics of large recurrent networks may inform the design of efficient methods for information retrieval and storage [5], [6]. Owing to a remarkable tradeoff between analytical tractability and explanatory power at multiple spatial scales, neural mass models are an ideal candidate for the design of control strategies. To replicate brain rhythms, neural mass models describe the evolution of population firing rates, which are obtained by filtering the population activations through nonlinear activation functions. In this work, we focus on the *rectifier* activation function, which defines the popular rectified linear units (ReLUs). Importantly, rectifiers possess wide-ranging biological relevance (as measured in sensory neurons [7]), and enable rich dynamics [8]–[10]. Our goal here is to identify efficient control strategies for interconnected neural populations with rectified linear activation functions. We characterize the reachability set of this ubiquitous class of models and exploit the piecewise nature of the rectified function to derive an array of results aimed at performing (feedback and feedforward) low-cost control in prototypical classes of networks with distinct connection types.

This work was supported by ONR grant N00014-18-1-2828. T. Menara and J. Cortés are with the Department of Mechanical and Aerospace Engineering, UC San Diego, {tmenara, cortes}@ucsd.edu.

Related work. The study of neural mass models has been a central theme in neuroscience since the early work of Wilson and Cowan, FitzHugh, and Schelter [8]. In this context, rectifier activation functions have been used since the 1960s as a common feature of rate models. Yet, only recent work performs formal analyses of these models with control-theoretic tools. The work [11] focuses on characterizing the stability properties of hierarchical (threshold-linear) rate models. The paper [12] investigates controllability of 2 and 3-dimensional rate models with sigmoidal activation functions (which can be approximated with rectifiers in certain regimes). Notwithstanding, a comprehensive control design for this class of models is still missing. From a dynamical systems standpoint, ReLUs display features of piecewise-linear and switching systems [13] (i.e., possess a piecewise-smooth flow with state and input-dependent switches), which yield a technically challenging control framework.

Paper contribution. The contribution[1] is twofold. First, we show that the positive orthant –which corresponds to firing rates operating in linear regime– is reachable from any positive initial condition. This result emphasizes the versatility of recurrent neural networks with rectifier activation function, and promotes the investigation of efficient control methods in diverse scenarios. Our second contribution focuses on this latter aspect. Specifically, we improve upon our first result by restricting our attention to pairs with population-specific connectivity, and present a series of control strategies that leverage the switch-affine nature of the system dynamics. Our strategies feature multiple benefits, such as constant and sparse inputs, straightforward extensions to larger networks, the characterization of systems and states associated with less cost to control, and practical relevance. We present both feedforward and feedback control strategies. The former finds application in biological settings [4], and the latter is useful in the context of reservoir computing [5]. For space reasons, all proofs are omitted and will appear elsewhere.

II. Problem setup and preliminary notions

This paper investigates control strategies for neural networks modeled by firing rate dynamics with rectified linear activation function. Our results are general, and are concerned with networks where the nodes represent either the

[1] We use $\mathbb{R}$, $\mathbb{R}_{\geq 0}$, and $\mathbb{R}_{>0}$ to denote the sets of real, nonnegative real, and positive real numbers, respectively. For $k \in \mathbb{R}$, the operator $\lceil k \rceil$ maps k to the least integer greater than or equal to k. We use bold letters for vectors and matrices. We use $\mathbf{I}$ for the identity matrix, and $\mathbf{0}$ for the zero vector. Further, v_i indicates the i-th component of a vector $\boldsymbol{v}$. If $\boldsymbol{x}$ and $\boldsymbol{y}$ are vectors, $\boldsymbol{x} \leq \boldsymbol{y}$ denotes $x_i \leq y_i$ for all i. Given $\boldsymbol{x} \in \mathbb{R}^n$, $\|\boldsymbol{x}\|$ is the 2-norm. We use the short-hand notation $\boldsymbol{x}^0 = \boldsymbol{x}(0)$ to indicate the initial state, and $\boldsymbol{x}^{\mathsf{f}}$ for the (target) state. Finally, $\mathbf{e}^i$ denotes the i-th canonical vector.

firing rate of a single neuron or the average firing rate of a population of neurons. Specifically, we consider a rate model of n interconnected nodes that obey the dynamics:

$$\dot{\boldsymbol{x}}(t) = -\boldsymbol{x}(t) + \phi(\mathbf{W}\boldsymbol{x}(t) + \mathbf{B}\boldsymbol{u}(t)), \quad \mathbf{0} \leq \boldsymbol{x}^0, \quad (1)$$

where $\boldsymbol{x} \in \mathbb{R}^n_{\geq 0}$ is the state of the system, i.e., the nodal firing rates, and the synaptic weights are encoded in the connectivity matrix $\mathbf{W} \in \mathbb{R}^{n\times n}$. The vector $\boldsymbol{u} \in \mathbb{R}^m$ represents an external input to the system, such as unmodeled background activity, an exogenous stimulus, a pattern to be learned, or an electromagnetic control signal. Inputs are administered to the network through an input matrix $\mathbf{B} \in \mathbb{R}^{n\times m}$. To model dedicated nodal inputs, we let $\mathcal{K} = \{k_1, \ldots, k_m\} \subseteq \{1, \ldots, n\}$ be the control set, and let $\mathbf{B} = [\mathbf{e}^{k_1}, \ldots, \mathbf{e}^{k_m}]$. Finally, the vector-valued function $\phi(\boldsymbol{y}) = \max(\mathbf{0}, \boldsymbol{y})$, where $\max(\cdot)$ is applied element-wise, defines a nonlinear response function that *rectifies* the thresholded excitatory responses to external inputs and the natural interactions with other nodes. In machine learning, $\phi(\cdot)$ defines the activation function of rectified linear units (ReLUs) [14].

It is worth noting that the rate model dynamics (1) partitions the phase plane into 2^n distinct regions [11], which are parameterized by a switching index $\boldsymbol{\sigma} \in \{0, \ell\}^n$. That is, $\sigma_i = 0$ if node i is inactive, and $\sigma_i = \ell$ if node i is in the linear regime. The switching of (1) is state and input-dependent, and the regions associated to $\boldsymbol{\sigma}$ are defined as:

$$\Omega_{\boldsymbol{\sigma}} = \{\boldsymbol{x} \in \mathbb{R}^n_{\geq 0} \ : \ (\mathbf{W}\boldsymbol{x} + \mathbf{B}\boldsymbol{u})_i \leq 0 \text{ if } \sigma_i = 0 \\ 0 < (\mathbf{W}\boldsymbol{x} + \mathbf{B}\boldsymbol{u})_i \text{ if } \sigma_i = \ell\}.$$

In light of this switching behavior, it is useful to consider (1) in the equivalent piecewise-affine form:

$$\dot{\boldsymbol{x}} = -(\mathbf{I} + \boldsymbol{\Sigma}\mathbf{W})\boldsymbol{x} + \boldsymbol{\Sigma}\mathbf{B}\boldsymbol{u} \qquad \forall \boldsymbol{x} \in \Omega_{\boldsymbol{\sigma}}, \qquad (2)$$

where the diagonal matrix $\Sigma = \Sigma(\boldsymbol{\sigma})$ satisfies $\Sigma_{ii} = 1$ if $\sigma_i = \ell$, and $\Sigma_{ii} = 0$ otherwise.

Despite possessing a seemingly "mild" nonlinearity, the control of networks with dynamics (1) is a challenging problem because (i) the input appears inside the nonlinearity, (ii) the vector field is state-dependent, as a single trajectory may cross multiple regions $\Omega_{\boldsymbol{\sigma}}$, and (iii) the regions $\Omega_{\boldsymbol{\sigma}}$ are parameter- and input-dependent (thus, typically time-varying). Moreover, even though (1) is also equivalent to a cone-wise linear system [15],[2] necessary and sufficient conditions for complete controllability[3] on $\mathbb{R}^n$ do not to hold. As the positive orthant is forward invariant with respect to the dynamics (1), in what follows we overcome the issues above and provide strategies to control state trajectories from and to states in $\mathbb{R}^n_{\geq 0}$. We make use of the notion of reachable sets to characterize which states can be reached in finite time.

Definition 1: ***(Reachable set)*** The *reachable set from* $\boldsymbol{x}^0$ for the rate dyanmics in (1) is the set of all states for which there exists $T \geq 0$ and an input $\boldsymbol{u} : [0, T] \to \mathbb{R}^m$ such that the solution $\boldsymbol{x}$ of (1) with $\boldsymbol{x}(0) = \boldsymbol{x}^0$ satisfies $\boldsymbol{x}(T)$. □

[2]Conewise form of (1): $\dot{\boldsymbol{x}} = -\mathbf{I}\boldsymbol{x} + \phi(\boldsymbol{y})$, with output $\boldsymbol{y} = \mathbf{W}\boldsymbol{x} + \mathbf{B}\boldsymbol{u}$.

[3]A system is completely controllable if for any pair of states $\boldsymbol{x}^0, \boldsymbol{x}^{\mathsf{f}}$, there exists a locally integrable input such that the solution to the systems dynamics can be steered to $\boldsymbol{x}(T) = \boldsymbol{x}^{\mathsf{f}}$ in a finite time $T > 0$.

In the remainder part of the paper, we show that we can design inputs to steer the state between any pair of initial and final states in the positive orthant. We then build upon this finding and investigate prototypical cases of inhibitory-inhibitory, excitatory-excitatory, and excitatory-inhibitory pairs to (i) discover whether sparse inputs (i.e., $\mathcal{K} \subsetneq \{1, \ldots, n\}$) affect the reachable set, (ii) design energy-efficient controllers, (iii) elucidate feedback and feedforward control approaches, and (iv) enact constant control inputs for situations where dynamical controllers may not be feasible.

III. Reachability analysis of neural populations with rectified linear activation function

This section introduces a control strategy to reach any target state in the open positive orthant. Our first result shows that no component can be driven to zero in finite time.

Lemma 3.1: ***(Zero components cannot be reached in finite time)*** Consider the rate dynamics (1) with initial condition $\boldsymbol{x}^0 \in \mathbb{R}^n_{>0}$. There does not exist a final time $T < \infty$ such that $x_i(T) = 0$ for any $i \in \{1, \ldots, n\}$.

We now show that there always exists an input that reaches any state in the open positive orthant in finite time.

Theorem 3.2: ***(Reachability of the positive orthant in finite time)*** The open positive orthant $\mathbb{R}^n_{>0}$ is a reachable set from any $\boldsymbol{x}^0 \in \mathbb{R}^n_{\geq 0}$ for the rate dynamics (1) with $\mathbf{B} = \mathbf{I}$. Moreover, given $\boldsymbol{x}^{\mathsf{f}} \in \mathbb{R}^n_{>0}$, there exists an input $\boldsymbol{u} : [0, T] \to \mathbb{R}^n$ such that $\boldsymbol{x}(T) = \boldsymbol{x}^{\mathsf{f}}$ with $T = 1$ if $2\boldsymbol{x}^{\mathsf{f}} \geq \boldsymbol{x}^0$, and $T = \lceil \log_2(\max_i(x_i^0/x_i^{\mathsf{f}})) \rceil$ otherwise.

The proof of Theorem 3.2 relies on the (iterative) application of the dynamical feedback controller

$$\boldsymbol{u}(t) = (\mathbf{I} - \mathbf{W})\boldsymbol{x}(t) + \boldsymbol{x}^{\mathsf{f}} - \boldsymbol{x}^0, \qquad (3)$$

to reach any target state in $\boldsymbol{x}^{\mathsf{f}} \in \mathbb{R}^n_{>0}$ from $\boldsymbol{x}^0 \in \mathbb{R}^n_{\geq 0}$ in finite time $T > 0$. As (3) generates a straight trajectory in the phase space, we refer to it as the *straight-line controller*. The following example illustrates some applications of the straight-line controller (3) in Theorem 3.2.

Example 1: ***(Applications of the straight-line controller)*** Consider $n = 3$ nodes with rate dynamics (1), $\mathbf{B} = \mathbf{I}$ and synaptic weights $\mathbf{W}$ as in Fig. 1(a). From $\boldsymbol{x}^0 = [3\ 3\ 3]^\top$, the application of (3) to reach a desired final firing rate $\boldsymbol{x}^{\mathsf{f}_1} = [7\ 4\ 6]^\top$ is illustrated in Fig. 1(b). If, instead, the desired firing rates are $\boldsymbol{x}^{\mathsf{f}_2} = [7\ 1\ 1.5]^\top$ (from the same initial state $\boldsymbol{x}^0$), it holds $2\boldsymbol{x}^{\mathsf{f}_2} < \boldsymbol{x}^0$. Therefore, we apply (3) to reach $\boldsymbol{x}^{\mathsf{i}} = (\boldsymbol{x}^0 + \boldsymbol{x}^{\mathsf{f}_2})/2$ first, and then again from $\boldsymbol{x}^{\mathsf{i}}$ to reach $\boldsymbol{x}^{\mathsf{f}_2}$. By applying (3) twice, we reach $\boldsymbol{x}^{\mathsf{f}_2}$ at a final time $T = 2$, in accordance with Theorem 3.2. □

A few comments are in order. Theorem 3.2 shows the reachability of the entire open positive orthant in finite time from any initial conditions in $\mathbb{R}^n_{\geq 0}$. However, if any component of $x_i^{\mathsf{f}} = 0$, then $T \to \infty$, consistently with Lemma 3.1. Clearly, the straight-line controller (3) can also be used to enforce and track any desired straight trajectory.

While the straight-line controller guarantees reaching any target state in a finite amount of time, its naïveté inherently presents a number of drawbacks. First, it assumes that n distinct inputs are available, i.e., $\mathbf{B} = \mathbf{I}$. Second, feedforward control laws may be preferable whenever the state cannot be

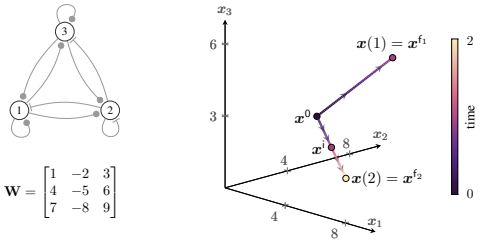

(a) (b)

Fig. 1: (a) The 3-node network in example 1 and its connectivity matrix $\mathbf{W}$. The network comprises 2 excitatory and 1 inhibitory unit and satisfies Dale's law (i.e., each column in $\mathbf{W}$ is either positive or negative). (b) This plot illustrates how the controller (3) steers the firing rate of the 3 nodes from $\boldsymbol{x}^0$ to $\boldsymbol{x}^{\mathrm{f}_1}$ and from $\boldsymbol{x}^0$ to $\boldsymbol{x}^{\mathrm{f}_2}$. The state trajectory is colored to emphasize its time evolution. Accordingly to Theorem 3.2, $\boldsymbol{x}(T_1) = \boldsymbol{x}^{\mathrm{f}_1}$ in time $T_1 = 1$. In regards to $\boldsymbol{x}^{\mathrm{f}_2}$, because it does not satisfy $2\boldsymbol{x}^{\mathrm{f}_2} \geq \boldsymbol{x}^0$, the same controller is used to reach the intermediate point $\boldsymbol{x}^{\mathrm{i}} = (\boldsymbol{x}^0 + \boldsymbol{x}^{\mathrm{f}_2})/2$ first, and then $\boldsymbol{x}^{\mathrm{f}_2}$, yielding a final time $T_2 = 2$.

continuously monitored. Third, there might be more energy efficient control laws that avoid canceling out the dynamics. Fourth and finally, in biological settings, the control method may require constant inputs (e.g., direct current stimulation [4]), thus constraining the control action.

In light of the above observations, the remainder of this paper focuses on developing control strategies for pairs (i.e., $n = 2$) of nodes with specific interconnection types. All in all, our analysis provides valuable insight that can be extended to larger networks (i.e., $n > 2$) and elucidates which parameters make the system "easier" to control.

IV. Control Strategies for Pairs of Rectified Linear Units

In this section, we restrict our attention to node pairs. Due to the relevance of Dale's law in biological neuronal networks [16],[4] we constrain the signs of each column in $\mathbf{W}$ to be either positive or negative. This choice gives rise to (i) purely inhibitory circuits, which regulate the activity of the auditory system [17], (ii) purely excitatory circuits, which are believed to promote the emergence of spontaneous activity in the retina, spinal cord, and hippocampus [18], and (iii) excitatory-inhibitory pairs, which have been shown to be especially relevant in the study of brain rhythms [10].

Before presenting our results, we emphasize that the main challenge in developing controllers for our model stems from the fact that the region boundaries between distinct regions $\Omega_{\boldsymbol{\sigma}}$ (cf. (2)) intimately depend on the input $\boldsymbol{u}$. As we are interested in efficient control methods, we measure the energy of a control input by

$$E(\boldsymbol{u}) = \int_0^T \|\boldsymbol{u}(\tau)\|^2 \mathrm{d}\tau. \tag{4}$$

Finally, because for $n = 2$ the phase plane is partitioned in 4 regions, we use $\Omega_{\ell\ell}$, $\Omega_{0\ell}$, $\Omega_{\ell 0}$, and Ω_{00} to denote the linear-linear ($\boldsymbol{\Sigma} = \mathbf{I}$), inactive-linear ($\boldsymbol{\Sigma} = [\mathbf{0},\ \mathbf{e}^2]$), linear-inactive ($\boldsymbol{\Sigma} = [\mathbf{e}^1,\ \mathbf{0}]$), and inactive-inactive regions ($\boldsymbol{\Sigma} = [\mathbf{0}\ \mathbf{0}]$).

A. Control of I-I pairs

We consider a pair of inhibitory nodes with dynamics (1) and synaptic weights $\mathbf{W} = \left[\begin{smallmatrix} -a & -b \\ -c & -d \end{smallmatrix}\right]$, with $a, b, c, d \in \mathbb{R}_{>0}$.

[4]Dale's law states that neurons that are excitatory (resp., inhibitory) only output excitatory (resp., inhibitory) signals.

TABLE I: Control strategies for I-I pairs

$(\boldsymbol{x}^0, \boldsymbol{x}^{\mathrm{f}})$ case	control strategy	result
$x_i^{\mathrm{f}} < x_i^0$ for some i	coasting, feedforward sparse, constant	Proposition 4.1
$\boldsymbol{x}^{\mathrm{f}} > \boldsymbol{x}^0$	feedforward, energy-efficient	Proposition 4.2

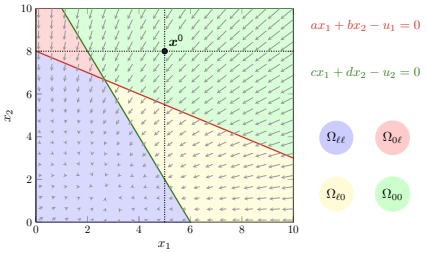

Fig. 2: Phase space of an I-I pair with parameters $a = d = 0.25$, $c = d = 0.5$, $\mathbf{B} = \mathbf{I}$, and constant control inputs $\boldsymbol{u} = [4\ 3]^\top$. The region boundaries are represented in red and green. The initial firing rates $\boldsymbol{x}^0$ further partition $\mathbb{R}^2_{\geq 0}$ into 4 affine subspaces which lend themselves to the design of distinct (tailored) control methods (see Table I). Notice that, for $\boldsymbol{u} = \mathbf{0}$, $\Omega_{00} = \mathbb{R}^2_{\geq 0}$. As $\boldsymbol{u} > 0$ becomes larger, the regions $\Omega_{\ell\ell}$, $\Omega_{0\ell}$, and $\Omega_{\ell 0}$ manifest in the positive orthant, as depicted here. Conversely, $\boldsymbol{u} < 0$ has no effect due to $\mathbf{W}\boldsymbol{x}$ being always negative for all $\boldsymbol{x} \in \mathbb{R}^2_{\geq 0}$ in $\phi(\cdot)$.

Fig. 2 illustrates the phase space properties of a controlled I-I pair. It is worth noting that, due to $\mathbf{W}\boldsymbol{x} < 0$ for all $\boldsymbol{x} \in \mathbb{R}^2_{\geq 0}$, any $\boldsymbol{u} < 0$ produces no effect on the dynamics. Table I summarizes the results of this section and the main advantages of the proposed control strategies. We distinguish between two cases: $\boldsymbol{x}^{\mathrm{f}} > \boldsymbol{x}^0$, and all other possibilities (i.e., $x_i^{\mathrm{f}} < x_i^0$ for some i). We start our treatment by focusing on the latter case, where we let one state *coast* along the vector flow while applying a single control input (i.e., $\mathcal{K} = \{1\}$ or $\mathcal{K} = \{2\}$) to steer the other state.

Proposition 4.1: ***(Control of I-I pairs when*** $x_i^{\mathrm{f}} < x_i^0$ ***by constant inputs and coasting)*** Consider an I-I pair with dynamics (1) and $\mathcal{K} = \{1\}$. Let $\mathcal{S}_1 = \{\boldsymbol{x} \ :\ x_2 \leq x_2^0 \text{ and } x_1 \geq (x_2^0/x_1^0)x_2\}$ and $T = -\log(x_2^{\mathrm{f}}/x_2^0)$. Any $\boldsymbol{x}^{\mathrm{f}} \in \mathcal{S}_1$ is reachable by applying

$$u_1 = \begin{cases} 0 & \text{if } 0 \leq t < t_1, \\ \bar{u}_1 \triangleq a\max(x_1^0, x_1^{\mathrm{f}}) + b\max(x_2^0, x_2^{\mathrm{f}}) & \text{if } t_1 \leq t \leq T, \end{cases}$$

if there exists $t_1 \geq 0$ solving

$$e^{-(a+1)T + at_1} x_1^0 + \tfrac{\bar{u}_1(1 - e^{-(a+1)(T-t_1)})}{a+1} - \tfrac{bx_2^0(e^{aT} - e^{at_1})}{a} = x_1^{\mathrm{f}}. \tag{5}$$

Otherwise, $\boldsymbol{x}^{\mathrm{f}}$ is reachable by applying

$$\bar{u}_1 = \frac{(a+1)\left(e^{-(a+1)T}x_1^0 - x_1^{\mathrm{f}} - \frac{bx_2^0}{a}(e^{aT} - 1)\right)}{e^{-(a+1)T} - 1} \tag{6}$$

for all $0 \leq t \leq T$.

In the interest of space, we only provide our results for $\mathcal{K} = \{1\}$, as a controller for the case $\mathcal{K} = \{2\}$ that reaches any $\boldsymbol{x}^{\mathrm{f}} \in \{\boldsymbol{x} \ :\ x_1 \leq x_1^0 \text{ and } x_2 \geq (x_1^0/x_2^0)x_1\}$ can be derived analogously to the one in Proposition 4.1. Notice that the controller designed in Proposition 4.1 is sparse and only requires to apply a constant value. That is, we do not need any state feedback to reach the final state, and we can do so by means of a single time-invariant control input. Finally, the choice of $\bar{u}_1$ so that $x_1 \in \Omega_{\ell 0}$ reveals which network parameters a and b are advantageous to steer the firing rate

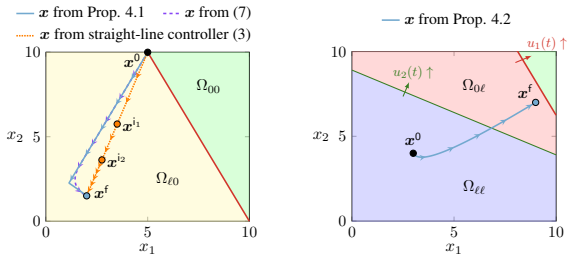

(a) (b)

Fig. 3: Control of the I-I pair with parameters as in Fig. 2. (a) Comparison of the trajectory from the controller $\bar{u}_1 = 5$ in Proposition 4.1 applied at $t_1 = 1.4888$ (in blue), the trajectory from the optimal time-varying controller computed from (7) (in purple, dashed), and the straight-line controller (3) (in orange, dotted). Both single-input controllers yield a qualitatively similar trajectory and require similar control energy ($E = 13.25$ for the one in Proposition 4.1, and $E = 10.88$ for (7)). To emphasize how $\boldsymbol{x} \in \Omega_{\ell 0}$ after the control $\bar{u}_1$ is turned on, the partitioning of $\mathbb{R}^2_{>0}$ by the regions $\Omega_{\ell 0}$ and Ω_{00} is shown for $t_1 \leq t \leq T$. The regions and regions boundaries are color-coded as in Fig. 2. Because $2\boldsymbol{x}^f > \boldsymbol{x}^0$ does not hold, the straight-line controller (3) is applied 3 times (requiring energy $E = 204.1$), and intermediate points $\boldsymbol{x}^{i_1}$,$\boldsymbol{x}^{i_2}$ are reached at $t = 1$ and $t = 2$, respectively. (b) Controller (8) applied to the same I-I pair to reach $\boldsymbol{x}^f = [9\ 7]^\top > \boldsymbol{x}^0$ in $T = 0.9$. The regions $\Omega_{\boldsymbol{\sigma}}$ are depicted at $\boldsymbol{u}(0) = [6.56\ 4.45]^\top$. As $\boldsymbol{u}(t)$ increases, the region boundaries (in red and green), shift to incorporate the entire trajectory in $\Omega_{\ell\ell}$.

with only one input. We can see from the definition of $\bar{u}_1$ that networks with $a \ll b$ require less energy (cf. (4)) to steer the system towards any $\boldsymbol{x}^f$ with small x_2^0 and large x_1^f.[5]

Remark 1: ***(Minimum-energy feedback control of I-I pairs)*** If the inputs are not constrained to be constant, then we can compute $\bar{u}_1$ in Proposition 4.1 by solving

$$\min_{u_1} \int_0^T |u_1(\tau)|^2 \mathrm{d}\tau \tag{7}$$
$$\text{s.t. } \dot{x}_1 = -(a+1)x_1 - bx_2^0 e^{-t} + u_1,$$
$$x_1(0) = x_1^0,\ x_1(T) = x_1^f,\ u_1(t) \geq ax_1(t) + bx_2^0 e^{-t},$$

which is convex, but requires measurements of $x_1(t)$. □

The next example compares the energy requirements of the controller in Proposition 4.1 to the ones of (3) and (7).

Example 2: ***(Comparison between controllers for an I-I pair)*** Consider the same I-I pair as in Fig. 2 with control set $\mathcal{K} = \{1\}$. We first apply the controller described in Proposition 4.1, which yields $\bar{u}_1 = 5$ applied at $t_1 = 1.4888 \leq t \leq T = 1.8971$. Next, we solve the problem in (7) with the YOP toolbox for Matlab [19]. The energy of $\bar{u}_1$ computed from Proposition 4.1 is $E(\bar{u}_1) = 13.25$. Instead, $u_1(t)$ from (7) yields $E(u_1(t)) = 10.88$. The two trajectories, which yield qualitatively similar results, are depicted in Fig. 3(a). The slightly higher control cost of $\bar{u}_1$ is counterbalanced by advantages such as being constant and feedforward. By allowing $\mathcal{K} = \{1, 2\}$, we also apply the straight-line controller (3). However, because $2\boldsymbol{x}^f < \boldsymbol{x}^0$, the controller achieves $\boldsymbol{x}(T) = \boldsymbol{x}^f$ at $T = 3$ after reaching two intermediate points $\boldsymbol{x}(1) = \boldsymbol{x}^{i_1}$ and $\boldsymbol{x}(2) = \boldsymbol{x}^{i_2}$. Finally, the controller (3) yields $E(\boldsymbol{u}) = 204.1$, which is 1 order of magnitude larger than the single-input controllers. □

Because control laws as the one in Proposition 4.1 allow us to control the pair's firing rate in all $\mathbb{R}^2_{>0} \setminus \{\boldsymbol{x} : \boldsymbol{x} > \boldsymbol{x}^0\}$, we conclude this section by investigating control laws for the case $\boldsymbol{x}^f > \boldsymbol{x}^0$. To present our result, we let $\mathbf{G}(t) = \int_0^t e^{(\mathbf{W}-\mathbf{I})^\top(\mathbf{W}-\mathbf{I})t}\mathrm{d}t$ be the controllability Gramian of dynamics (1) with $\mathcal{K} = \{1, 2\}$ in $\Omega_{\ell\ell}$ [20].

Proposition 4.2: ***(Control of I-I pairs when $\boldsymbol{x}^f > \boldsymbol{x}^0$)*** Consider an I-I pair with dynamics (1) and control set $\mathcal{K} = \{1, 2\}$. There always exists $T > 0$ such that $\boldsymbol{x}(T) = \boldsymbol{x}^f$ for any pair $(\boldsymbol{x}^0, \boldsymbol{x}^f) \in \mathbb{R}^{2\times 2}_{>0}$ with $\boldsymbol{x}^f > \boldsymbol{x}^0$ by the controller

$$\boldsymbol{u}(t) = -e^{(\mathbf{W}-\mathbf{I})^\top(T-t)}\mathbf{G}(t)^{-1}(e^{(\mathbf{W}-\mathbf{I})T}\boldsymbol{x}^0 - \boldsymbol{x}^f). \tag{8}$$

Fig. 3(b) illustrates an application of (8). Note that (8) is a minimizer of

$$\min_{\boldsymbol{u}} \int_0^T \|\boldsymbol{u}(\tau)\|^2 \mathrm{d}\tau \tag{9}$$
$$\text{s.t. } \dot{\boldsymbol{x}} = (\mathbf{W}-\mathbf{I})\boldsymbol{x}(t) + \mathbf{B}\boldsymbol{u}(t),\ \boldsymbol{x}(0) = \boldsymbol{x}^0,\ \boldsymbol{x}(T) = \boldsymbol{x}^f.$$

Therefore, amongst all the controllers that keep $\boldsymbol{x}(t) \in \Omega_{\ell\ell}$ at all times, which is a sufficient condition to reach any $\boldsymbol{x}^f > \boldsymbol{x}^0$, (8) is the most energy efficient. Numerical simulations suggest that (8) is also the minimum-energy control for (1) when T is sufficiently small and $\boldsymbol{x}^f > \boldsymbol{x}^0$. However, computing the final time T for which this holds is beyond the scope of this paper. We conclude this section by observing that Proposition 4.2 immediately extends to networks of $n > 2$ nodes.

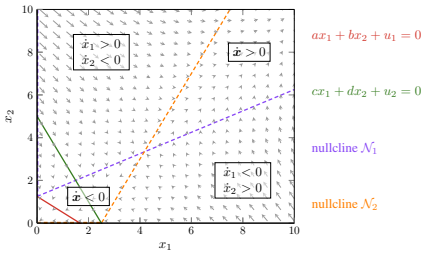

Fig. 4: Phase space of an E-E pair with parameters $a = 0.6$, $b = 0.8$, $c = 1$, $d = 0.5$, $\mathbf{B} = \mathbf{I}$, and constant control inputs $\boldsymbol{u} = [-1\ \ -2.5]^\top$. The region boundaries are represented in red and green. To not clutter the figure, we choose not to highlight the regions $\Omega_{\boldsymbol{\sigma}}$. Notice that $\mathrm{sign}(\dot{\boldsymbol{x}}_i)$ switches whenever $\boldsymbol{x}$ crosses the nullclines $\mathcal{N}_1$ and $\mathcal{N}_2$ (in dashed purple and orange, respectively.

B. Control of E-E pairs

Next, we turn our attention to a pair of excitatory nodes with dynamics (1) and synaptic weights $\mathbf{W} = \left[\begin{smallmatrix} a & b \\ c & d \end{smallmatrix}\right]$, with $a, b, c, d \in \mathbb{R}_{>0}$. Notice that any $\boldsymbol{u}(t) > 0$ yields $\boldsymbol{x}(t) \in \boldsymbol{\Omega}_{\ell\ell}$ at all times. Besides distinguishing between different relative locations of $\boldsymbol{x}^0$ and $\boldsymbol{x}^f$, we shall also distinguish between E-E pairs with $a, d > 1$, and E-E pairs with $0 < a \leq 1$ or $0 < d \leq 1$. In the former case, there are no nullclines $\mathcal{N}_i \triangleq \{\boldsymbol{x} : \dot{x}_i = 0\}$ that cross $\mathbb{R}^2_{>0}$ for any value of $\boldsymbol{u} > 0$. Instead, in the latter case, nullclines typically intersect $\mathbb{R}^2_{>0}$ even in the absence of control. Fig. 4 illustrates the complexity of the phase space of an E-E pair.

We start by presenting control strategies for pairs with $a, d > 1$. Table II summarizes our control strategies.

Proposition 4.3: ***(Control of E-E pairs when $\boldsymbol{x}^f > \boldsymbol{x}^0$)*** Consider an E-E pair with dynamics (1), $a, d > 1$, and control set $\mathcal{K} = \{1, 2\}$. For any $T > 0$ such that $e^{(\mathbf{W}-\mathbf{I})T}\boldsymbol{x}^0 < \boldsymbol{x}^f$, the controller (8) achieves $\boldsymbol{x}(T) = \boldsymbol{x}^f$.

[5]The same reasoning leads to preferring $c \ll d$ when steering the system with $\mathcal{K} = \{2\}$ to any $\boldsymbol{x}^f$ with large x_2^f and small x_1^0.

TABLE II: Control strategies for E-E pairs with $a, d > 1$

$(\boldsymbol{x}^0, \boldsymbol{x}^{\mathrm{f}})$ case	control strategy	result
$\boldsymbol{x}^{\mathrm{f}} > \boldsymbol{x}^0$	feedforward, energy-efficient	Proposition 4.3
	feedforward, sparse, constant	Remark 2
$x_i^{\mathrm{f}} < x_i^0$ for one i	feedforward, constant	Proposition 4.4
$\boldsymbol{x}^{\mathrm{f}} < \boldsymbol{x}^0$	feedback, faster than (3)	Proposition 4.5

Proposition 4.3 emphasizes that specific values of $\boldsymbol{x}^0$ and $\boldsymbol{x}^{\mathrm{f}}$ allow us to exploit the dynamics in $\boldsymbol{\Omega}_{\ell\ell}$ to use (8). Moreover, the only condition is to set a final time T small enough to guarantee that the input remains positive.

Proposition 4.4: ***(Control of E-E pairs when $x_i^0 < x_i^{\mathrm{f}}$ by constant inputs)*** Consider an E-E pair with dynamics (1), $a, d > 1$, and control set $\mathcal{K} = \{1, 2\}$. Suppose $x_2^{\mathrm{f}} < x_2^0$ and $x_1^{\mathrm{f}} > x_1^0$, and let $T = -\log(x_2^{\mathrm{f}}/x_2^0)$. The controller $\bar{\boldsymbol{u}}$ with $\bar{u}_1 = \dfrac{(a-1)\left(e^{(a-1)T}x_1^0 - x_1^{\mathrm{f}} - \frac{bx_2^0}{a}(e^T - e^{(a-1)T})\right)}{e^{(a-1)T}-1}$, $\bar{u}_2 = -cx_1^{\mathrm{f}} - dx_2^0$, achieves $\boldsymbol{x}(T) = \boldsymbol{x}^{\mathrm{f}}$ if $\bar{u}_1 > -ax_1^{\mathrm{f}} - bx_2^0$.

The same reasoning can be used to design a controller for $\boldsymbol{x}^{\mathrm{f}}$ with $x_2^{\mathrm{f}} > x_2^0$ and $x_1^{\mathrm{f}} < x_1^0$, and is omitted here. With respect to synaptic weights that lower the energy needed to control the system, $|\bar{u}_2|$ becomes smaller (thus decreasing $\|\bar{\boldsymbol{u}}\|$) if $c \ll 1$ when $x_1^{\mathrm{f}} \gg 1$, or if $d \ll 1$ when $x_2^0 \gg 1$. We are left with the case $\boldsymbol{x}^{\mathrm{f}} < \boldsymbol{x}^0$, which we treat next.

Proposition 4.5: ***(Feedback control of E-E pairs when $\boldsymbol{x}^{\mathrm{f}} < \boldsymbol{x}^0$)*** Consider an E-E pair with dynamics (1), $a, d > 1$, and control set $\mathcal{K} = \{1, 2\}$. Suppose $\boldsymbol{x}^{\mathrm{f}} < \boldsymbol{x}^0$, and let $T_i = -\log(x_i^{\mathrm{f}}/x_i^0)$, $i \in \{1, 2\}$. There always exists a controller $\tilde{\boldsymbol{u}}$ of the form

$$\tilde{\boldsymbol{u}}(t) = -\mathbf{W}\boldsymbol{x}(t) + \bar{\boldsymbol{u}}, \tag{10}$$

with constant $\bar{\boldsymbol{u}} \geq 0$ that achieves $\boldsymbol{x}(T) = \boldsymbol{x}^{\mathrm{f}}$ in $T = \min(T_1, T_2)$. Moreover, $\bar{\boldsymbol{u}}$ can be chosen as

$$\bar{\boldsymbol{u}} = \begin{cases} \left[0 \;\; (x_2^{\mathrm{f}} - e^{-T}x_2^0)/(1-e^{-T})\right]^\top & \text{if } T_1 < T_2, \\ \left[(x_1^{\mathrm{f}} - e^{-T}x_1^0)/(1-e^{-T}) \;\; 0\right]^\top & \text{otherwise.} \end{cases}$$

It is worth noting that due to the final time T depending on a natural logarithm instead of a logarithm in base 2, the controller (10) achieves $\boldsymbol{x}(T) = \boldsymbol{x}^{\mathrm{f}}$ faster than (3).

Remark 2: ***(Sparse control inputs in E-E pairs)*** Differently from pairs with inhibitory connections, E-E pairs with $a, d > 1$ are more challenging to control with sparse inputs. However, in the case of $\boldsymbol{x}^{\mathrm{f}} > \boldsymbol{x}^0$, a single control input can be designed in the same fashion as the one in Proposition 4.1. In fact, a controller applied to node i with $i = \arg\max_{i\in\{1,2\}} -\log(x_i^{\mathrm{f}}/x_i^0)$ ensures $\boldsymbol{x}(T) = \boldsymbol{x}^{\mathrm{f}}$. □

We now briefly touch upon E-E pairs with $a < 1$ and/or $d < 1$. Whenever either $a < 1$ or $d < 1$, and $x_i^{\mathrm{f}} > x_i^0$ for some i, constant controllers can be designed analogously to Proposition 4.4. Further, in the case $\boldsymbol{x}^{\mathrm{f}} < \boldsymbol{x}^0$, feedback controllers can be designed analogously to Proposition 4.5. More interesting E-E pairs possess both $a, d < 1$, where we can exploit the sign shift in $\dot{\boldsymbol{x}}$ between the nullclines, see Fig. 4. Table III summarizes our results in this case.

Proposition 4.6: ***(Control of E-E pairs with $a, d < 1$ when $\boldsymbol{x}^{\mathrm{f}} > \boldsymbol{x}^0$ by constant inputs)*** Consider an E-E pair with dynamics (1), $a, d < 1$, and control set $\mathcal{K} = \{1, 2\}$. Suppose $\boldsymbol{x}^{\mathrm{f}} > \boldsymbol{x}^0$. The constant controller

$$\bar{\boldsymbol{u}} = (\mathbf{I} - e^{(\mathbf{W}-\mathbf{I})T})^{-1}(\mathbf{W} - \mathbf{I})\left(e^{(\mathbf{W}-\mathbf{I})T}\boldsymbol{x}^0 - \boldsymbol{x}^{\mathrm{f}}\right) \tag{11}$$

TABLE III: Control strategies for E-E pairs with $a, d < 1$

$(\boldsymbol{x}^0, \boldsymbol{x}^{\mathrm{f}})$ case	control strategy	features
$\boldsymbol{x}^{\mathrm{f}} > \boldsymbol{x}^0$	feedforward, constant	Proposition 4.6
$\boldsymbol{x}^{\mathrm{f}} < \boldsymbol{x}^0$	feedforward, constant	Proposition 4.7
other cases	feedforward, constant	Proposition 4.4

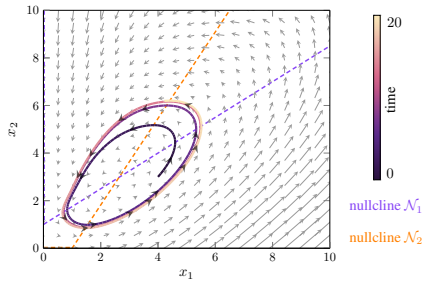

Fig. 5: Phase space for $a = 2.5$, $b = c = 2$, $d = 0.1$ and constant input $\boldsymbol{u} = [2 \;\; -2]^\top$. Because the weights and the input satisfy (12), there is a unique unstable equilibrium $\boldsymbol{x}^* = [2.638 \;\; 2.979]^\top$ (as in (13)) in $\Omega_{\ell\ell}$ at the intersection of the two nullclines. The state trajectory plotted in this figure reveals the limit cycle orbit.

achieves $\boldsymbol{x}(T) = \boldsymbol{x}^{\mathrm{f}}$ for all T such that $\bar{\boldsymbol{u}} > 0$.

We reason that, for constant controllers such as the one in Proposition 4.6, systems with $\frac{1-a}{b} > \frac{c}{1-d}$ require a higher cost (i.e., higher $\|\bar{\boldsymbol{u}}\|$). To see this, rewrite the nullclines as $x_2 = \frac{1-a}{b} - \frac{u_1}{b}$ and $x_2 = \frac{c}{1-d} + \frac{u_2}{1-d}$, and notice that $\dot{\boldsymbol{x}} < 0$ whenever the slope of the former line is larger than the slope of the second one (see Fig. 4). The converse holds for the case $\boldsymbol{x}^{\mathrm{f}} < \boldsymbol{x}^0$, which we address next.

Proposition 4.7: ***(Control of E-E pairs with $a, d < 1$ when $\boldsymbol{x}^{\mathrm{f}} < \boldsymbol{x}^0$ by constant inputs)*** Consider an E-E pair with dynamics (1), $a, d < 1$, and control set $\mathcal{K} = \{1, 2\}$. Suppose $\boldsymbol{x}^{\mathrm{f}} > \boldsymbol{x}^0$. The constant controller (11) achieves $\boldsymbol{x}(T) = \boldsymbol{x}^{\mathrm{f}}$ for all T such that $\bar{\boldsymbol{u}} > -\mathbf{W}\boldsymbol{x}^{\mathrm{f}}$.

We conclude this section by emphasizing that controllers akin to the one in Proposition 4.4 can be used to achieve $\boldsymbol{x}(T) = \boldsymbol{x}^{\mathrm{f}}$ in the cases $x_i^0 < x_i^{\mathrm{f}}$, $x_{-i}^0 < x_{-i}^{\mathrm{f}}$.

C. Control of E-I pairs

We are now ready to address pairs of one excitatory neuron and one inhibitory neuron. The with synaptic weights satisfy $\mathbf{W} = \left[\begin{smallmatrix} a & -b \\ c & -d \end{smallmatrix}\right]$, with $a, b, c, d \in \mathbb{R}_{>0}$. In general, we can adapt the control strategies developed above to E-I pair. In the interests of space, we focus on what sets E-I pairs apart: the existence of isolated attractive orbits in the phase space – that is, limit cycles. In the following, we assume $\mathcal{K} = \{1, 2\}$.

It is a known result that all solutions to (1) (except the one originating from the unique unstable equilibrium in (13)) converge to a limit cycle if and only if [10], [21]:

$$d+2 < a, \;\; (a-1)(d+1) < bc, \;\; u_1 > 0, \;\; u_2 < \tfrac{(d+1)u_1}{d}. \tag{12}$$

If (12) holds, the system has a unique unstable equilibrium

$$\boldsymbol{x}^* = \frac{1}{bc - (1+d)(a-1)}\begin{bmatrix}(1+d)u_1 - bu_2 \\ cu_1 - (a-1)u_2\end{bmatrix}. \tag{13}$$

Fig. 5 illustrates the emergence of a limit cycle.

The above conditions provide a novel control opportunity: hitching a ride on the limit cycle. Because the region boundaries $x_2 = \frac{a}{b}x_1 + \frac{u_1}{b}$ and $x_2 = \frac{c}{d}x_1 + \frac{u_2}{d}$ increase their x_2-coordinate as $\boldsymbol{u} > 0$ becomes larger, there always exists $T > 0$ such that $\boldsymbol{u} > 0$ as in (8) reaches $\boldsymbol{x}^{\mathrm{f}} > \boldsymbol{x}^0$ (akin

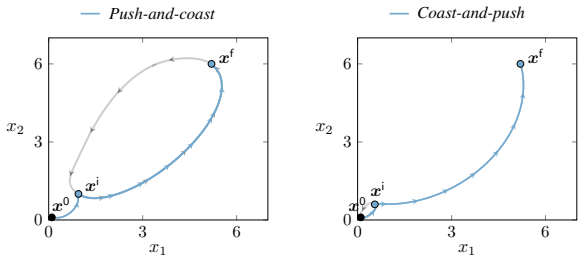

Fig. 6: Left, application of the *push-and-coast* control strategy in an E-I pair with $a = 2.5$, $b = c = 2$, $d = 0.1$. The controller (8) is used for $T^{\mathsf{ME}} = 0.6$ to reach from $\boldsymbol{x}^0 = [0.1\ 0.1]^\top$ the closest point $\boldsymbol{x}^{\mathsf{i}} = [0.95\ 1]^\top$ in the limit cycle associated to $\boldsymbol{u}^{\mathsf{LC}} = [2\ \ -2]^\top$ (in gray). The latter input is applied until $\boldsymbol{x}(T^{\mathsf{ME}} + T^{\mathsf{LC}} = 2.67) = \boldsymbol{x}^{\mathsf{f}} = [5.2\ 6]^\top$. The total energy required is $E^{\mathsf{ME}} + E^{\mathsf{LC}} = 7.43$. Right, application of the *coast-and-push* strategy in the same E-I pair of the left panel with the same $\boldsymbol{x}^0$, $\boldsymbol{x}^{\mathsf{f}}$. Here, $\boldsymbol{u}^{\mathsf{LC}} = [0.2\ \ -0.22]^\top$ is applied for $T^{\mathsf{LC}} = 2.06$, and (8) is applied for $T^{\mathsf{ME}} = 0.6$. The total energy required is $E^{\mathsf{ME}} + E^{\mathsf{LC}} = 58.41$, which is 7.86 times more energy than the *push-and-coast* strategy for this pair $(\boldsymbol{x}^0, \boldsymbol{x}^{\mathsf{f}})$.

to Proposition 4.2). For the sake of simplicity, we restrict our analysis to this case, and suppose that the attractive closed orbit $\gamma_{\boldsymbol{x}^*}$ associated to $\boldsymbol{x}^*$ is known. We let $\boldsymbol{u}^{\mathsf{LC}} = (\mathbf{I}-\mathbf{W})\boldsymbol{x}^*$ denote the control input associated to $\boldsymbol{x}^*$ in (13). We propose two control strategies to combine minimum-energy control and limit-cycle coasting. In both strategies, $\boldsymbol{x}^*$ is such that $\boldsymbol{x}^0 \leq \min_{\boldsymbol{x}\in\gamma_{\boldsymbol{x}^*}} \boldsymbol{x} < \max_{\boldsymbol{x}\in\gamma_{\boldsymbol{x}^*}} \boldsymbol{x} \leq \boldsymbol{x}^{\mathsf{f}}$ (i.e., the limit cycle lies between $\boldsymbol{x}^0$ and $\boldsymbol{x}^{\mathsf{f}}$).

1) Push-and-coast: Step (i): Utilize (8) to reach $\boldsymbol{x}^{\mathsf{i}} = \min_{\boldsymbol{x}\in\gamma_{\boldsymbol{x}^*}} \|\boldsymbol{x} - \boldsymbol{x}^0\|$, where $\boldsymbol{x}^*$ is such that $\boldsymbol{x}^{\mathsf{f}} \in \gamma_{\boldsymbol{x}^*}$. Step (ii): apply $\boldsymbol{u}^{\mathsf{LC}}$ until $\boldsymbol{x}(T) = \boldsymbol{x}^{\mathsf{f}}$.

2) Coast-and-push: Step (i): utilize $\boldsymbol{u}^{\mathsf{LC}}$ with $\boldsymbol{x}^*$ such that $\boldsymbol{x}^0 \in \gamma_{\boldsymbol{x}^*}$ until $\boldsymbol{x}(t) = \min_{\boldsymbol{x}\in\gamma_{\boldsymbol{x}^*}} \|\boldsymbol{x} - \boldsymbol{x}^{\mathsf{f}}\|$. Step (ii) Apply (8) to reach $\boldsymbol{x}(T) = \boldsymbol{x}^{\mathsf{f}}$.

Given $(\boldsymbol{x}^0, \boldsymbol{x}^{\mathsf{f}})$, to find which control strategy requires the least energy, we let T^{ME} denote the time during which the minimum-energy control (8) is applied, T^{LC} denote the time during which $\boldsymbol{u}^{\mathsf{LC}}$ keeps the limit cycle active, $E^{\mathsf{ME}} = T^{\mathsf{ME}}(\boldsymbol{x}^{\mathsf{f}} - e^{(\mathbf{W}-\mathbf{I})T^{\mathsf{ME}}}\boldsymbol{x}^0)^\top \mathbf{G}^{-1}(T^{\mathsf{ME}})(\boldsymbol{x}^{\mathsf{f}} - e^{(\mathbf{W}-\mathbf{I})T^{\mathsf{ME}}}\boldsymbol{x}^0)$ be the energy associated with (8) [20], and $E^{\mathsf{LC}} = T^{\mathsf{LC}}\|\boldsymbol{u}^{\mathsf{LC}}\|$ the energy associated with $\boldsymbol{u}^{\mathsf{LC}}$. Clearly, the control strategy requiring the least energy is the one that minimizes $E^{\mathsf{ME}} + E^{\mathsf{LC}}$. Fig. 6 compares them both. Notice that, in both panels, the *push* control is guaranteed to be positive (thus, $\boldsymbol{x}(t) \in \Omega_{\ell\ell}$) by $\boldsymbol{x}^{\mathsf{f}} > \boldsymbol{x}^0$. Whenever the latter inequality is not satisfied, the controller (8) may yield $\boldsymbol{x}(t) \notin \Omega_{\ell\ell}$.

Remark 3: ***(Control of E-I pair with $\boldsymbol{x}^0 < \boldsymbol{x}^{\mathsf{f}}$ by limit cycle)*** The push-and-coast control strategy can be simplified if there exists $0 < t_1 < \infty$ with $\{\boldsymbol{x}(t_1) = e^{(\mathbf{W}-\mathbf{I})t_1}\boldsymbol{x}^0\} \cap \gamma_{\boldsymbol{x}^*} \neq \emptyset$ from any $\boldsymbol{x}^0, \boldsymbol{x}(t_1) \in \Omega_{\ell\ell}$ for $\boldsymbol{u} = 0$. I.e., if $\boldsymbol{x}(t) = e^{(\mathbf{W}-\mathbf{I})t}\boldsymbol{x}^0$ intersects the limit cycle orbit, then the only input needed to reach $\boldsymbol{x}^{\mathsf{f}}$ is $\boldsymbol{u}^{\mathsf{LC}}$. This simplification agrees with empirical observations of neural circuitry efficiently exploiting limit cycle attractors during memory tasks [22].□

V. Conclusions

This paper presents control strategies for rate models of interconnected neural units with rectified activation function. We show that there exists a controller capable of steering the network state between any pair of initial and final states in the (open) positive orthant in finite time. Furthermore, by focusing on interconnected pairs, we present feedforward and feedback control strategies that feature constant input signals, sparse controllers, and low control energy. Directions of future research include an exhaustive investigation of limit-cycle coasting strategies and the application of the results to the training of recurrent neural networks.

References

[1] S. Ching and J. Ritt. Control strategies for underactuated neural ensembles driven by optogenetic stimulation. *Frontiers in Neural Circuits*, 7, 2013.

[2] T. Menara, G. Lisi, F. Pasqualetti, and A. Cortese. Brain network dynamics fingerprints are resilient to data heterogeneity. *Journal of Neural Engineering*, 18(2):026004, 2021.

[3] S. Pequito, A. Ashourvan, D. S. Bassett, B. Litt, and G. J. Pappas. Spectral control of cortical activity. In *American Control Conference*, pages 2785–2791, Seattle, WA, USA, 2017.

[4] J. Stiso, A. N. Khambhati, T. Menara, A. E. Kahn, J. M. Stein, S. R. Das, R. Gorniak, J. Tracy, B. Litt, K. A. Davis, F. Pasqualetti, T. H. Lucas, and D. S. Bassett. White matter network architecture guides direct electrical stimulation through optimal state transitions. *Cell Reports*, 28(10):2554 – 2566.e7, 2019.

[5] Z. Lu and D. S. Bassett. Invertible generalized synchronization: A putative mechanism for implicit learning in neural systems. *Chaos: An Interdisciplinary Journal of Nonlinear Science*, 30(6):063133, 2020.

[6] L. E. Suárez, B. A. Richards, G. Lajoie, and B. Misic. Learning function from structure in neuromorphic networks. *Nature Machine Intelligence*, 3(9):771–786, 2021.

[7] N. J. Priebe and D. Ferster. Direction selectivity of excitation and inhibition in simple cells of the cat primary visual cortex. *Neuron*, 45(1):133–145, 2005.

[8] P. Dayan and L. F. Abbott. *Theoretical Neuroscience: Computational and Mathematical Modeling of Neural Systems*. Computational Neuroscience. MIT Press, Cambridge, MA, 2001.

[9] E. Nozari and J. Cortés. Hierarchical selective recruitment in linear-threshold brain networks. Part II: Inter-layer dynamics and top-down recruitment. *IEEE Transactions on Automatic Control*, 66(3):965–980, 2021.

[10] F. Celi, A. Allibhoy, F. Pasqualetti, and J. Cortés. Linear-threshold dynamics for the study of epileptic events. *IEEE Control Systems Letters*, 5(4):1405–1410, 2021.

[11] E. Nozari and J. Cortés. Hierarchical selective recruitment in linear-threshold brain networks. Part I: Intra-layer dynamics and selective inhibition. *IEEE Transactions on Automatic Control*, 66(3):949–964, 2021.

[12] S. A. Kim and S. Ching. Quasilinearization-based controllability analysis of neuronal rate networks. In *American Control Conference*, pages 7371–7376, Boston, MA, Jul 2016.

[13] M. K. J. Johansson. *Piecewise linear control systems: a computational approach*, volume 284. Springer, 2003.

[14] X. Glorot, A. Bordes, and Y. Bengio. Deep sparse rectifier neural networks. In *Proceedings of the fourteenth international conference on artificial intelligence and statistics*, pages 315–323. JMLR Workshop and Conference Proceedings, 2011.

[15] M. K. Camlibel, W. P. M. H. Heemels, and J. M. Schumacher. Algebraic necessary and sufficient conditions for the controllability of conewise linear systems. *IEEE Transactions on Automatic Control*, 53(3):762–774, 2008.

[16] J. C. Eccles. From electrical to chemical transmission in the central nervous system: the closing address of the sir Henry Dale centennial symposium. *Notes and records of the Royal Society of London*, 30(2):219–230, 1976.

[17] K. Kandler. Activity-dependent organization of inhibitory circuits: lessons from the auditory system. *Current Opinion in Neurobiology*, 14(1):96–104, 2004.

[18] M. B. Feller. Spontaneous correlated activity in developing neural circuits. *Neuron*, 22(4):653–656, 1999.

[19] V. Leek. An optimal control toolbox for MATLAB based on CasADi. Master's thesis, Linköping University, Vehicular Systems, 2016.

[20] T. Kailath. *Linear Systems*. Prentice-Hall, 1980.

[21] E. Nozari and J. Cortés. Oscillations and coupling in interconnections of two-dimensional brain networks. In *2019 American Control Conference (ACC)*, pages 193–198, Philadelphia, PA, 2019.

[22] E. Ghazizadeh and S. Ching. Slow manifolds within network dynamics encode working memory efficiently and robustly. *PLOS Computational Biology*, 17(9):1–20, 09 2021.